An Anisotropic Gurson Yield Criterion for Porous Ductile Sheet Metals with Planar Anisotropy

D.-A. Wang*, J. Pan* and S.-D. Liu**

**Mechanical Engineering*
The University of Michigan, Ann Arbor, MI 48109, USA

***Technical Research Center*
National Steel Company, Trenton, MI 48183, USA

January 12, 2003

Abstract

The influence of plastic anisotropy on the plastic behavior of porous ductile materials is investigated by a three-dimensional finite element analysis. A unit cell of cube containing a spherical void is modeled. The Hill quadratic anisotropic yield criterion is used to describe the matrix anisotropy including planar anisotropy. The matrix material is first assumed to be elastic perfectly plastic. Macroscopically uniform displacements are applied to the faces of the cube. The finite element computational results are compared with those based on the closed-form anisotropic Gurson yield criterion (Liao et al., *Mech. Mater.* 1997, pp. 213-226) in terms of an average anisotropy parameter. Three fitting parameters are used in the closed-form anisotropic Gurson yield criterion to fit the results of finite element computations. When the strain hardening of the matrix is considered, the computational results of the macroscopic stress-strain behavior are in agreement with those based on the closed-form anisotropic Gurson yield criterion under selected monotonically increasing loading conditions.

1. Introduction

Accurate description of the plastic behavior and ductile failure processes of sheet metals under biaxial loading conditions is necessary for accurate prediction of the failure in sheet metal forming processes. Ductile failure processes in metals usually involve nucleation, growth and coalescence of microvoids. Microvoids may nucleate due to the existence of second phase particles. These particles may separate from the surrounding matrix material or these particles may break and create microvoids. Microvoids then grow by plastic deformation and finally coalesce to form microcracks. In order to model the plastic flow and failure of these ductile materials, Gurson (1977) conducted an upper bound analysis of simplified models containing voids and proposed an approximate yield criterion for porous materials where the matrices obey the von Mises yield criterion. Tvergaard (1981, 1982) introduced three additional fitting parameters in Gurson's yield criterion by comparing the results of shear band instability in square arrays of cylindrical holes and axisymmetric spherical voids based on finite element models with those based on Gurson's yield criterion.

The matrix material in the original Gurson model was assumed to be isotropic in general in many research works on plastic localization and fracture analysis. However, sheet metals for stamping applications usually display certain extent of plastic anisotropy due to cold or hot rolling processes. In general, an average value of the anisotropy parameter R is used to characterize the sheet anisotropic plastic behavior. Here, R is defined as the ratio of the transverse plastic strain rate to the through-thickness plastic strain rate under in-plane uniaxial loading conditions. Numerous anisotropic yield criteria have been proposed over years (for example, see Hill, 1948, 1979; Gotoh, 1977; Budianski, 1984; Logan and Hosford, 1980; Bassani, 1977; Barlat et al., 1991, 1997).

Liao et al. (1997) first investigated the effects of the matrix normal anisotropy on the macroscopic plastic behavior of porous materials. In the work of Liao et al. (1997), a simplified sheet model containing a through-thickness hole under plane stress conditions was considered. The matrix material normal anisotropy was characterized by Hill's quadratic anisotropic yield criterion (Hill, 1948) and Hill's non-quadratic anisotropic yield criterion (Hill, 1979). An upper bound analysis was carried out and the numerical results can be fitted by a closed-form macroscopic yield criterion. An anisotropic Gurson yield criterion for sheet metals with spherical voids based on Hill's quadratic anisotropic yield criterion (Hill, 1948) was also proposed. Note that Chen et al. (2001) also proposed an anisotropic Gurson yield criterion based on the higher-order yield criterion of Barlat et al. (1991) for aluminum sheet metals.

In this paper, a three-dimensional finite element analysis of a cube containing a spherical void is carried out to test the applicability of the anisotropic Gurson yield criterion proposed by Liao et al. (1997) for voided solids with planar anisotropy. Since sheet metals under forming operations are usually under plane stress conditions, the unit cell of a cube is assumed to be mainly subjected to plane stress conditions. The analysis is performed for various void volume fractions as well as different average R values. As in Tvergaard (1981, 1982), the anisotropic Gurson yield criterion is modified by adding three fitting parameters to fit the results based on the modified yield criterion with the finite element computational results when the matrix is assumed to be perfectly plastic. Finite element computations with consideration of the matrix strain hardening under proportional straining conditions are also performed. The results of finite element

simulations are compared with those based on the unmodified and modified anisotropic Gurson yield criterion. Finally, discussions and conclusions are given.

2. Hill Quadratic Anisotropic Yield Criterion

Sheet metals usually have plastic anisotropy including planar anisotropy after rolling processes. Many anisotropic yield criteria have been proposed to characterize the plastic anisotropy. In this investigation, we adopt Hill's quadratic anisotropic yield criterion (Hill, 1948). The Yld96 yield criterion (Barlat et al., 1997) is another candidate yield criterion to characterize plastic anisotropy for full stress states. However, numerical difficulties have been encountered in finite element applications for implementation of the yield criterion (Yoon et al., 2000). Figure 1 shows an element of sheet metal and a Cartesian coordinate system. The Cartesian coordinates coincide with the orthotropy symmetry axes of the sheet metal. Here, X_1 represents the rolling direction, X_2 represents the transverse direction, and X_3 represents the thickness direction. Hill's quadratic anisotropic yield criterion ϕ (Hill, 1948) can be written as

$$\phi = F(\sigma_{22} - \sigma_{33})^2 + G(\sigma_{33} - \sigma_{11})^2 + H(\sigma_{11} - \sigma_{22})^2$$
$$+ 2L\sigma_{23}^2 + 2M\sigma_{31}^2 + 2N\sigma_{12}^2 - \sigma_0^2 = 0 \qquad (1)$$

where σ_{ij} are the stresses, σ_0 represents a reference yield stress, *F, G, H, L, M,* and *N* are material constants. We can use tensile and shear tests with respect to different orientations to determine the material constants. In this investigation, the values of R obtained from tensile tests at different in-plane orientations with respect to the rolling direction are used to characterize the plastic anisotropy. The values of R usually vary with the orientation of the tensile axis. Here, σ_0 is taken as the yield stress in the rolling

direction. We can express the material constants *F, G, H, L, M,* and *N* in terms of the anisotropy parameters R_0, R_{45}, and R_{90} which represent the values of R when the tensile axis is at 0°, 45°, and 90° from the rolling (X_1) direction, respectively. In this investigation, the material constants *L, M,* and *N* related to the shear responses of σ_{23}, σ_{31} and σ_{12} in the yield criterion are taken to be identical according to the computational results of the anisotropic plastic behavior of sheet metals after plane strain compression using a polycrystal model for b.c.c. metals as reported in Liao et al. (1998). Other values of material constants associated with σ_{31} and σ_{23} can be assigned when experimental data are available. Then the yield criterion in Equation (1) can be rewritten as

$$\phi = \frac{1}{1+R_0}\left[\frac{R_0}{R_{90}}(\sigma_{22}-\sigma_{33})^2 + (\sigma_{33}-\sigma_{11})^2 + R_0(\sigma_{11}-\sigma_{22})^2 \right.$$

$$\left. + \frac{(2R_{45}+1)(R_0+R_{90})}{R_{90}}(\sigma_{23}^2+\sigma_{31}^2+\sigma_{12}^2)\right] - \sigma_0^2 = 0 \qquad (2)$$

The detailed derivation of Equation (2) can be found in Appendix A. When the planar isotropy is considered, $R_0 = R_{45} = R_{90} = R$. Here, R can be considered as the normal anisotropy parameter. Then the yield criterion becomes

$$\phi = \frac{1}{1+R}\left[(\sigma_{22}-\sigma_{33})^2 + (\sigma_{33}-\sigma_{11})^2 + R(\sigma_{11}-\sigma_{22})^2 \right.$$

$$\left. + 2(2R+1)(\sigma_{23}^2+\sigma_{31}^2+\sigma_{12}^2)\right] - \sigma_0^2 = 0 \qquad (3)$$

3. Anisotropic Gurson Yield Criterion

Liao et al. (1997) derived an anisotropic Gurson yield criterion for a circular thin disk with a through thickness hole using an upper bound analysis. The matrix

surrounding the hole was assumed to be rigid perfectly plastic, incompressible and rate insensitive. Hill's quadratic anisotropic yield criterion (Hill, 1948) and Hill's non-quadratic anisotropic yield criterion (Hill, 1979) were used to describe the matrix normal anisotropy and planar isotropy. Liao et al. (1997) obtained a closed-form macroscopic yield criterion based on Hill's quadratic anisotropic yield criterion under axisymmetric loading conditions for the thin disk with a through thickness hole. A modified Gurson yield criterion Φ_R was proposed in Liao et al. (1997) for normal anisotropic sheet metals with spherical voids as

$$\Phi_R = \left(\frac{\Sigma_e}{\sigma_o}\right)^2 + 2q_1 f \cosh\left(q_2 \sqrt{\frac{1+2R}{6(1+R)}} \frac{3\Sigma_m}{\sigma_o}\right) - 1 - q_3 f^2 = 0 \tag{4}$$

where Σ_e represents the macroscopic effective stress, σ_o is the matrix yield stress under in-plane uniaxial loading conditions, f is the void volume fraction, R is the anisotropic parameter to characterize the normal anisotropy, Σ_m is the macroscopic mean stress, and q_1, q_2, and q_3 are the fitting parameters which are determined by a finite element analysis of a unit cell with a spherical void by Chien et al. (2001). The macroscopic effective stress Σ_e is expressed in terms of the macroscopic stresses Σ_{ij} based on Hill's quadratic anisotropic yield criterion in Equation (3) as

$$\Sigma_e = \left\{\frac{1}{1+R}\left[(\Sigma_{22}-\Sigma_{33})^2 + (\Sigma_{33}-\Sigma_{11})^2 + R(\Sigma_{11}-\Sigma_{22})^2 \right.\right.$$

$$\left.\left. + 2(2R+1)(\Sigma_{23}^2 + \Sigma_{31}^2 + \Sigma_{12}^2)\right]\right\}^{1/2} \tag{5}$$

The macroscopic mean stress Σ_m is

$$\Sigma_m = \frac{\Sigma_{11} + \Sigma_{22} + \Sigma_{33}}{3} \tag{6}$$

For sheet metals, $\overline{R}$ is usually used to characterize the average planar anisotropy. Here, $\overline{R}$ is defined as

$$\overline{R} = \frac{R_0 + 2R_{45} + R_{90}}{4} \tag{7}$$

In order to have a Gurson-type yield criterion for porous materials with consideration of planar plastic anisotropy, we propose to modify Equation (4) by replacing R by $\overline{R}$ as

$$\Phi = \left(\frac{\Sigma_e}{\sigma_o}\right)^2 + 2q_1 f \cosh\left(q_2 \sqrt{\frac{1+2\overline{R}}{6(1+\overline{R})}} \frac{3\Sigma_m}{\sigma_o}\right) - 1 - q_3 f^2 = 0 \tag{8}$$

where the macroscopic effective stress Σ_e is defined as in Equation (2) as

$$\Sigma_e = \left\{ \frac{1}{1+R_0} \left[\frac{R_0}{R_{90}} \left(\Sigma_{22} - \Sigma_{33}\right)^2 + \left(\Sigma_{33} - \Sigma_{11}\right)^2 + R_0 \left(\Sigma_{11} - \Sigma_{22}\right)^2 \right.\right.$$

$$\left.\left. + \frac{\left(2R_{45}+1\right)\left(R_0 + R_{90}\right)}{R_{90}} \left(\Sigma_{23}^2 + \Sigma_{31}^2 + \Sigma_{12}^2\right) \right] \right\}^{1/2} \tag{9}$$

In this paper, we conduct finite element computations of a unit cell with a spherical void under various combined loading conditions to investigate whether the anisotropic Gurson yield criterion proposed in Equation (8) can be used to describe the plastic flow of the porous materials, where the matrix plastic flow is based on Hill's quadratic anisotropic yield criterion (Hill, 1948) with in-plane plastic anisotropy as specified by R_0, R_{45} and R_{90}.

4. Finite Element Model

A porous ductile material containing a triply periodic array of spherical voids is considered here to investigate the plastic behavior of porous ductile materials. Because

of the regular arrangement of the voids, the porous ductile material containing a triply periodic array of spherical voids can be modeled by considering a unit cell of the cube with a spherical void at its center, as shown in Figure 2(a). The Cartesian coordinates X_1, X_2, and X_3 perpendicular to the cube faces are also shown in the figure. The Cartesian coordinates coincide with the material orthotropic symmetry axes. Note that the relative dimensions of a unit cell in the three directions can affect the plastic behavior of the unit cell (Pardeon and Hutchinson, 2000). In this paper, we concentrate on the effects of plastic anisotropy of the matrix and therefore a unit cell of a cube is taken for consideration. For demonstration of the finite element mesh, only one eighth of a finite element mesh used for computations is shown in Figure 2(b). Note that unlike the one-sixteenth cube model used in Hom and McMeeking (1989) and Jeong and Pan (1995), we adopt the entire cell model to properly take account for the planar plastic anisotropy. The void surface is specified to have zero traction. Macroscopically uniform displacements are applied on the faces so that the outer faces of the unit cell remain planes during the deformation.

To take the planar anisotropy into account, we consider three different loading scenarios with the principal loading direction at 0°, 45°, and 90° from the rolling direction of the sheet metals. Uniform normal displacements ΔX_1, ΔX_2, and ΔX_3 in the X_1, X_2, and X_3 directions are applied on the cell faces perpendicular to the X_1, X_2, and X_3 directions, respectively. For the principal loading direction at 0° from the rolling direction of the sheet metal, the relative uniform normal displacements applied to the faces of the unit cell are listed in Table 1. Five straining conditions with different displacement ratios are considered: equal-triaxial, equal-biaxial, plane strain, nearly

uniaxial ($\Delta X_2 / \Delta X_1 = -1/2$), and nearly pure shear ($\Delta X_2 / \Delta X_1 = -1$). The displacement ratios are assigned according to the small-strain rigid isotropic plasticity convention. In this table, "not prescribed" means that the surface remains planar without any specified nodal force or displacement. For the principal loading direction at 90° from the rolling direction of the sheet metal, the relative uniform normal displacements applied to the faces of the unit cell are listed in Table 2. For the principal loading direction at 45° from the rolling direction of the sheet metal, the mesh of the unit cell is rotated 45° with respect to the X_3 direction while the plastic orthotropic symmetry planes remain unchanged. For this loading direction, the relative uniform normal displacements applied to the faces of the unit cell are the same as those of the cases with the principal loading direction at 0° from the rolling direction. In all loading cases at different principal loading directions, the symmetry planes of plastic orthotropy remain unchanged.

The matrix material is assumed to be elastic perfectly plastic. We consider a high strength steel and an aluminum used as benchmark materials in the Numisheet'93 conference. The material properties of the steel and the aluminum are listed in Table 3. Several initial void volume fractions (f = 0.01, 0.04, 0.09 and 0.12) are considered here to examine the applicability of the proposed yield criterion in Equation (8). Hill's quadratic anisotropic yield criterion ϕ in Equation (2) is used to describe the matrix material with planar anisotropy.

The commercial finite element program ABAQUS (Hibbitt et al., 2001) is used to perform the computations. Under different loading conditions, the macroscopic stresses are calculated by averaging the surface tractions acting on the faces of the unit cell. The macroscopic yield point is defined as the limited stress state where massive plastic

deformation occurs. The corresponding macroscopic effective stress Σ_e in Equation (9) and macroscopic mean stress Σ_m in Equation (6) are then calculated and compared with those based on the anisotropic Gurson yield criterion in Equation (8).

In addition to the elastic perfectly plastic material model employed to calculate the fully plastic limits, the macroscopic plastic flow characteristics due to the matrix strain hardening are investigated under proportional nearly uniaxial and equal-biaxial tensile loading conditions. The relative uniform normal displacements applied to the faces of the unit cell are based on the normality flow rule and the yield criterion for the matrix as in Equation (2) under uniaxial and equal-biaxial conditions. The ratios of the normal displacement applied to the faces of the unit cell are listed in Table 4. The matrix effective tensile stress σ_M as a function of the effective tensile strain ε_M^p can be expressed as

$$\sigma_M = C_1(C_2 + \varepsilon_M^p)^{C_3} \tag{10}$$

where $C_1 = 677.16$ MPa, $C_2 = 0.01129$, and $C_3 = 0.2186$ for the high strength steel, and $C_1 = 570.40$ MPa, $C_2 = 0.01502$, and $C_3 = 0.3469$ for the aluminum. These material constants are base on the tensile stress-strain relation in the rolling direction as specified by the Numisheet'93 conference.

5. Numerical Results

Finite element computational results are used to evaluate the applicability of the use of the anisotropic Gurson yield criterion in Equation (8) to model the macroscopic anisotropic plastic behavior of porous materials. We examine the computational results for porous materials with elastic perfectly plastic matrices. For several different void

volume fractions (f = 0.01, 0.04, 0.09 and 0.12), Figures 3(a-f) show the computational results, represented by symbols, for the steel and the aluminum with principal loading directions at 0°, 45°, and 90° from the rolling direction, respectively. In these figures, both the macroscopic mean stresses and the macroscopic effective stresses are normalized by the matrix yield stress σ_o in the rolling direction. For comparison, various forms of curves based on the unmodified anisotropic Gurson yield criterion ($q_1 = q_2 = q_3 = 1$) in Equation (8) are also shown for different void volume fractions. As shown in the figures, when the void volume fraction is small, the finite element computational results are in agreement with those based on the unmodified anisotropic Gurson yield criterion. However, when the void volume fraction is large, the yield contours based on the unmodified anisotropic Gurson yield criterion are much larger than those of the finite element computations when the normalized mean stress Σ_m/σ_0 is low. When the normalized mean stress Σ_m/σ_0 is high under equal-triaxial loading conditions, the unmodified anisotropic Gurson yield criterion underestimate the yield behavior of the steel whereas the unmodified anisotropic Gurson yield criterion overestimate the yield behavior of the aluminum. Therefore, three fitting parameters q_1, q_2 and q_3 are needed in the anisotropic Gurson yield criterion as suggested by Liao et al. (1997).

Figures 4(a-f) show the computational results, represented by symbols, and the results, represented by various forms of curves, based on the modified anisotropic Gurson yield criterion with the selections of the fitting parameters q_1 = 1.45, q_2 = 0.81 and q_3 = 1.6 for the steel and q_1 = 1.45, q_2 = 0.95 and q_3 = 1.6 for the aluminum, respectively. For the steel, the value of q_2 is different from that suggested by Chien et al. (2001) for steels, but the values of q_1 and q_3 are the same as those in Chien et al. (2001) for steels. The

values of q_1, q_2, and q_3 for the aluminum are the same as those suggested by Chien et al. (2001) for aluminums. Note that an increase of q_1 can lower the predicted macroscopic yield stresses of the anisotropic Gurson yield criterion. The parameter q_2 has the effect on the weighting of the macroscopic mean stresses. In general, q_2 can be taken at a value of about 1 for a wide range of circumstances. An increase of q_3 will move up the yield contour in the $\Sigma_m/\sigma_o - \Sigma_e/\sigma_o$ plot, and the influence of q_3 will become more significant when the void volume fraction is large. With the fitting parameters, the curves based on the modified anisotropic Gurson yield criterion agree much better with the finite element computational results. As shown in Figure 4, the modified anisotropic Gurson yield criterion with the average $\overline{R}$ can be used to predict the yielding of porous ductile materials under the major principal loading conditions at 0°, 45°, and 90° from the rolling direction of the sheet metals. It should be noted that when the unit cell is subjected to in-plane nearly pure shear and plane strain tension, the macroscopic effective stresses from our finite element computations are slightly lower than those predicted by the modified anisotropic Gurson yield criterion. The reason for the earlier yielding can be attributed to the shear localization in the matrix material.

In order to explore further the accuracy of the use of the modified anisotropic Gurson yield criterion to predict the macroscopic plastic hardening behavior of porous materials, the macroscopic plastic hardening relations from finite element computations are compared with those based on the unmodified ($q_1 = q_2 = q_3 = 1$) and modified anisotropic Gurson yield criterion. Note that the values of the material constants are listed in Table 3 and the matrix strain hardening relation is expressed in Equation (10) for the steel and the aluminum. Figures 5 and 6 show the normalized macroscopic stress as a

function of the macroscopic tensile strain under nearly uniaxial tensile conditions for the steel and the aluminum, respectively. Figures 7 and 8 show the normalized macroscopic effective stress as a function of the macroscopic tensile strain under nearly equal-biaxial tensile conditions for the steel and the aluminum, respectively. Note that we use the normality flow rule and the yield criterion for the matrix to determine the relative displacement ratios of the faces of the unit cell. From the computational results, the macroscopic transverse normal stresses remain nearly zero under nearly uniaxial tension cases, whereas the in-plane macroscopic stresses are nearly equal to each other under nearly equal biaxial loading conditions. In Figures 5-8, E_{11}, E'_{11}, and E_{22} represent the macroscopic tensile strain in the 0°, 45°, and 90° directions, respectively. Also Σ_{11}, Σ'_{11}, and Σ_{22} represent the macroscopic tensile stress in the 0°, 45°, and 90° directions, respectively. The macroscopic stresses Σ_{11}, Σ'_{11}, and Σ_{22} are normalized by the yield stress σ_0, σ_{45}, and σ_{90} which represent the matrix yield stresses in the 0°, 45°, and 90° directions, respectively. The value of σ_0 is determined by setting $\varepsilon_M^p = 0$ in Equation (10). The values of σ_{45} and σ_{90} are then obtained by substituting the values of σ_0, R_0, R_{45} and R_{90} into the yield criterion in Equation (2) for the loading in the 45° and 90° directions, respectively.

For f = 0.01, Figures 5(a-c) and 6(a-c) show the macroscopic stress-strain relations based on the finite element computational results and those based on the modified and unmodified anisotropic Gurson yield criterion for the steel and the aluminum under nearly uniaxial tensile conditions, respectively. The governing equations based on the anisotropic Gurson yield criterion for the macroscopic plastic

behavior of porous materials with consideration of the matrix strain hardening are summarized in Appendix B. For the steel as shown in Figures 5(a-c), the finite element computational results agree well with those based on the modified anisotropic Gurson yield criterion for the loading in the 0° and 90° directions but slightly less than those based on the modified anisotropic Gurson yield criterion for the loading in the 45° direction. For the aluminum shown in Figures 6(a-c), the finite element computational results in general agree well with those based on the modified anisotropic Gurson yield criterion.

For $f = 0.09$, Figures 5(d-f) and 6(d-f) show the computational results and macroscopic stress-strain relations based on the anisotropic Gurson yield criterion for the steel and the aluminum, respectively. These figures show that for both the steel and aluminum the finite element computational results agree well with those based on the modified anisotropic Gurson yield criterion at small strains for the loading in the 0° and 90° directions. As the strain becomes large, the computational results agree well with those based on the unmodified anisotropic Gurson yield criterion. For the steel, when the loading is in the 45° direction, the finite element computational results are slightly lower than those based on the modified anisotropic Gurson yield criterion at small strains. When the strain becomes large, the computational results agree with those based on the modified anisotropic yield criterion. For the aluminum, when the loading is in the 45° direction, the computational results agree well with those based on the modified anisotropic Gurson yield criterion. When the strain becomes large, the computational results fall between those based on the modified and unmodified anisotropic Gurson yield criterion.

Figures 7 and 8 show the macroscopic stress-strain relations in the X_1 and X_2 directions based on the finite element computational results and those based on the modified and unmodified anisotropic Gurson yield criterion under nearly equal-biaxial tensile loading conditions. The macroscopic stresses Σ_{11} and Σ_{22} are normalized by σ_b which is determined by substituting the values of σ_0, R_0, R_{45} and R_{90} into the yield criterion in equation (2) under equal biaxial stress conditions. For a small void volume fraction (f = 0.01), the computational results agree with those based on the unmodified anisotropic Gurson yield criterion as shown in Figures 7(a-b) and 8(a-b). For a large void volume fraction (f = 0.09), the computational results agree with those based on the unmodified anisotropic Gurson yield criterion as shown in Figures 7(c-d) and 8(c-d).

6. Conclusions and Discussions

A unit cell of a cube containing a spherical void is modeled by a finite element analysis to validate the anisotropic Gurson yield criterion proposed by Liao et al. (1997) to characterize the plastic behavior of porous material with planar anisotropic matrices. The plastic anisotropic behavior of the matrices is described by Hill's quadratic anisotropic yield criterion. The matrix material is assumed to be elastic perfectly plastic. The results of the finite element computations indicate that the finite element results for the steel and the aluminum subjected to the major principal loads at 0°, 45° and 90° from the rolling direction of the sheet metal can be fitted reasonably well by those based on the modified anisotropic Gurson yield criterion in terms of the average anisotropy parameter $\overline{R}$ with suggested fitting parameters. When the matrix plastic hardening behavior is considered, we found that the macroscopic plastic hardening relations based on the finite

element computations and the unmodified anisotropic Gurson yield criterion are in good agreement for the steel and the aluminum under nearly uniaxial and equal-biaxial loading conditions. Therefore, based on the limited computational results obtained in this investigation, the proposed anisotropic Gurson yield criterion in Equations (8), (9), and (6) can be a reasonable candidate to be used to investigate the anisotropic behavior of porous materials with the matrices characterized by Hill's quadratic anisotropic yield criterion.

Acknowledgement

This work was initiated through a summer internship for D.-A. Wang at National Steel Technical Center in 2001. The support of National Steel for this work is appreciated.

Appendix A: Hill's quadratic anisotropic yield criterion

Hill's quadratic anisotropic yield criterion (1948) can be written as

$$\phi = F(\sigma_{22}-\sigma_{33})^2 + G(\sigma_{33}-\sigma_{11})^2 + H(\sigma_{11}-\sigma_{22})^2$$
$$+ 2L\sigma_{23}^2 + 2M\sigma_{31}^2 + 2N\sigma_{12}^2 - \sigma_0^2 = 0 \tag{A1}$$

Based on the associated flow rule, the plastic strain rates $\dot{\varepsilon}_{11}^p$, $\dot{\varepsilon}_{22}^p$, $\dot{\varepsilon}_{33}^p$, and $\dot{\varepsilon}_{12}^p$ can be obtained as

$$\dot{\varepsilon}_{11}^p = \dot{\lambda}\frac{\partial\phi}{\partial\sigma_1} = \dot{\lambda}\left[-2G(\sigma_{33}-\sigma_{11}) + 2H(\sigma_{11}-\sigma_{22})\right] \tag{A2}$$

$$\dot{\varepsilon}_{22}^p = \dot{\lambda}\frac{\partial\phi}{\partial\sigma_2} = \dot{\lambda}\left[2F(\sigma_{22}-\sigma_{33}) - 2H(\sigma_{11}-\sigma_{22})\right] \tag{A3}$$

$$\dot{\varepsilon}_{33}^p = \dot{\lambda}\frac{\partial\phi}{\partial\sigma_3} = \dot{\lambda}\left[-2F(\sigma_{22}-\sigma_{33}) + 2G(\sigma_{33}-\sigma_{11})\right] \tag{A4}$$

$$2\dot{\varepsilon}_{12}^p = \dot{\lambda}\frac{\partial\phi}{\partial\sigma_{12}} = \dot{\lambda}\left[4N\sigma_{12}\right] \tag{A5}$$

where $\dot{\lambda}$ is a scalar factor of proportionality.

We first consider a uniaxial loading in the X_1 direction which is at 0° from the rolling direction. In this case, $\sigma_{11} \neq 0$, $\sigma_{22} = \sigma_{33} = \sigma_{23} = \sigma_{31} = \sigma_{12} = 0$, R_0 can be obtained as

$$R_0 = \frac{\dot{\varepsilon}_{22}^p}{\dot{\varepsilon}_{33}^p} = \frac{H}{G} \tag{A6}$$

Then we consider a uniaxial loading in the X_2 direction which is at 90° from the rolling direction. In this case, $\sigma_{22} \neq 0$, $\sigma_{11} = \sigma_{33} = \sigma_{23} = \sigma_{31} = \sigma_{12} = 0$, R_{90} can be obtained as

$$R_{90} = \frac{\dot{\varepsilon}_{11}^p}{\dot{\varepsilon}_{33}^p} = \frac{H}{F} \tag{A7}$$

Consider the coordinate system rotates 45° counterclockwise with respect to the X_3 axis to a new coordinate system of X_1', X_2', and X_3'. Now we consider a uniaxial loading in the X_1' direction with respect to the rolling direction. In this case, the stress transformation gives the stress components with respect to the X_1, X_2, and X_3 coordinates as $\sigma_{11} = \sigma_{22} = \sigma_{12} = \sigma/2$, and $\sigma_{33} = \sigma_{31} = \sigma_{23} = 0$. Here, σ represents the tensile stress. The plastic strain rates can be obtained from Equations (A2), (A3), and (A5) as

$$\varepsilon_{11}^{p} = \dot{\lambda} G \sigma \tag{A8}$$

$$\dot{\varepsilon}_{22}^{p} = \dot{\lambda} F \sigma \tag{A9}$$

$$\dot{\varepsilon}_{12}^{p} = \dot{\lambda} N \sigma \tag{A10}$$

Based on the strain transformation, the plastic transverse plastic strain rate $\dot{\varepsilon}_{22}'^{p}$ with respect to the coordinate system of X_1', X_2', and X_3' is

$$\dot{\varepsilon}_{22}'^{p} = \dot{\lambda} \frac{1}{2} \left[G\sigma + F\sigma - 2N\sigma \right] \tag{A11}$$

Since $\dot{\varepsilon}_{33}'^{p} = \dot{\varepsilon}_{33}^{p}$, we can write the through-thickness plastic strain rate $\dot{\varepsilon}_{33}'^{p}$ with respect to the coordinate system of X_1', X_2', and X_3' as

$$\dot{\varepsilon}_{33}'^{p} = \dot{\lambda} \left[-F\sigma - G\sigma \right] \tag{A12}$$

Therefore, R_{45} can be written as

$$R_{45} = \frac{\dot{\varepsilon}_{22}'^{p}}{\dot{\varepsilon}_{33}'^{p}} = \frac{2N - (F+G)}{2(F+G)} \tag{A13}$$

As mentioned before, we take σ_0 in Equation (A1) as the yield stress in the X_1 direction. Then

$$G + H = 1 \tag{A14}$$

We can solve for F, G, H, and N using Equations (A6), (A7), (A13), and (A14) as

$$F = \frac{R_0}{R_{90}\left(1 + R_0\right)} \tag{A15}$$

$$G = \frac{1}{1 + R_0} \tag{A16}$$

$$H = \frac{R_0}{1 + R_0} \tag{A17}$$

$$N = \frac{\left(2R_{45} + 1\right)\left(R_0 + R_{90}\right)}{2R_{90}\left(1 + R_0\right)} \tag{A18}$$

Substituting Equations (A15) - (A18) into (A1) and assuming $L = M = N$ give the yield criterion in Equation (2).

Appendix B: Macroscopic plastic behavior of porous ductile materials with consideration of the matrix strain hardening

We consider monotonically increasing proportional deformation histories such as monotonically increasing nearly uniaxial and equal-biaxial tensile conditions where the principal directions of the macroscopic deformation do not change. The macroscopic strain rate tensor $\dot{E}_{ij}$ can be decomposed into an elastic part $\dot{E}^e_{ij}$ and a plastic part $\dot{E}^p_{ij}$.

$$\dot{E}_{ij} = \dot{E}^e_{ij} + \dot{E}^p_{ij} \tag{B1}$$

The elastic macroscopic strain rates $\dot{E}^e_{ij}$ are related to the macroscopic stress rates $\dot{\Sigma}_{ij}$ as

$$\dot{E}^e_{ij} = \frac{1}{E^*}\left(\left(1+\nu^*\right)\delta_{ik}\delta_{jl} - \nu^*\delta_{ij}\delta_{kl}\right)\dot{\Sigma}_{kl} \tag{B2}$$

where E^* and ν^* represent the effective Young's modulus and Poisson's ratio of the porous material (Tandon and Weng, 1988). E^* and ν^* are expressed in terms of Young's modulus E and Poisson's ratio ν of the matrix material as

$$\begin{aligned} E^* &= \frac{2E(7-5\nu)(1-f)}{14-10\nu+f(1+\nu)(13-15\nu)}, \\ \nu^* &= \frac{\nu(14-10\nu)+f(1+\nu)(3-5\nu)}{14-10\nu+f(1+\nu)(13-15\nu).} \end{aligned} \tag{B3}$$

For porous materials with the matrix strain hardening, the modified anisotropic Gurson yield criterion in Equation (8) is written here again as

$$\Phi = \left(\frac{\Sigma_e}{\sigma_M}\right)^2 + 2q_1 f\cosh\left(q_2\sqrt{\frac{1+2\overline{R}}{6(1+\overline{R})}}\frac{3\Sigma_m}{\sigma_M}\right) - 1 - q_3 f^2 = 0 \tag{B4}$$

where σ_M represents the matrix flow stress. The matrix strain hardening is specified in Equation (10). The macroscopic plastic strain rates $\dot{E}^p_{ij}$ are determined by the associated flow rule as

$$\dot{E}_{ij}^{p} = \dot{\Lambda}\frac{\partial \Phi}{\partial \Sigma_{ij}} \tag{B5}$$

where $\dot{\Lambda}$ is a scalar factor of proportionality.

Due to the plastic incompressibility of the matrix material, the growth rate of the void volume fraction, $\dot{f}$, can be related to the macroscopic plastic dilatational strain rate $\dot{E}_{kk}^{p}$ as

$$\dot{f} = (1-f)\dot{E}_{kk}^{p} \tag{B6}$$

The equivalence of macroscopic plastic work rate and microscopic plastic dissipation rate gives

$$\Sigma_{ij}\dot{E}_{ij}^{p} = (1-f)\sigma_{M}\dot{\varepsilon}_{M}^{p} \tag{B7}$$

Equation (B7) can be rewritten as

$$\Sigma_{ij}\dot{E}_{ij}^{p} = \frac{1}{h}(1-f)\sigma_{M}\dot{\sigma}_{M} \tag{B8}$$

where $h = d\sigma_{M} / d\varepsilon_{M}^{p}$.

The consistency condition is expressed as

$$\dot{\Phi} = \frac{\partial \Phi}{\partial \Sigma_{ij}}\dot{\Sigma}_{ij} + \frac{\partial \Phi}{\partial \sigma_{M}}\dot{\sigma}_{M} + \frac{\partial \Phi}{\partial f}\dot{f} = 0 \tag{B9}$$

Combining the above equations, the macroscopic stress rates can be expressed in terms of the macroscopic strain rates.

For uniaxial tension applied at 0° from the rolling direction, $\Sigma_{22} = \Sigma_{33} = 0$. Therefore, $\Sigma_{e} = \Sigma_{11}$ and $\Sigma_{kk} = 3\Sigma_{m} = \Sigma_{11}$. We first solve the initial value of Σ_{11} from the macroscopic yield criterion in Equation (B4) for a given f and σ_{M} (= σ_{o}). With the initial conditions, rate equations are needed to determine the evolution of the

macroscopic stresses Σ_{ij}, the matrix flow stress σ_M, and the void volume fraction *f*. From Equation (B5), the macroscopic plastic strain rates $\dot{E}^p_{11}$, $\dot{E}^p_{22}$ and $\dot{E}^p_{33}$ can be obtained as

$$\dot{E}^p_{11} = \dot{\Lambda}\frac{\partial \Phi}{\partial \Sigma_{11}} = \dot{\Lambda}\left[\frac{2\Sigma_{11}}{\sigma_M^2} + 2q_1 f \sinh\left(Q_2\frac{\Sigma_{11}}{\sigma_M}\right)\frac{Q_2}{\sigma_M}\right] \tag{B10}$$

$$\dot{E}^p_{22} = \dot{\Lambda}\frac{\partial \Phi}{\partial \Sigma_{22}} = \dot{\Lambda}\left[\frac{-R_0}{1+R_0}\frac{2\Sigma_{11}}{\sigma_M^2} + 2q_1 f \sinh\left(Q_2\frac{\Sigma_{11}}{\sigma_M}\right)\frac{Q_2}{\sigma_M}\right] \tag{B11}$$

$$\dot{E}^p_{33} = \dot{\Lambda}\frac{\partial \Phi}{\partial \Sigma_{33}} = \dot{\Lambda}\left[\frac{-1}{1+R_0}\frac{2\Sigma_{11}}{\sigma_M^2} + 2q_1 f \sinh\left(Q_2\frac{\Sigma_{11}}{\sigma_M}\right)\frac{Q_2}{\sigma_M}\right] \tag{B12}$$

where $Q_2 = q_2\sqrt{\frac{1+2\overline{R}}{6\left(1+\overline{R}\right)}}$. For a prescribed $\dot{E}^p_{11}$, the scalar factor $\dot{\Lambda}$ can be solved from Equation (B10). Once $\dot{\Lambda}$ is solved, $\dot{E}^p_{22}$ and $\dot{E}^p_{33}$ can be obtained. Then the macroscopic plastic dilatational strain rate $\dot{E}^p_{kk}$ can be determined as

$$\dot{E}^p_{kk} = \dot{\Lambda}\frac{\partial \Phi}{\partial \Sigma_{kk}} = \dot{\Lambda}\left[6q_1 f \sinh\left(Q_2\frac{\Sigma_{11}}{\sigma_M}\right)\frac{Q_2}{\sigma_M}\right] \tag{B13}$$

Substituting Equation (B13) into Equation (B6) gives the growth rate of the void volume fraction, $\dot{f}$. For uniaxial tension at 0° from the rolling direction, Equation (B8) becomes

$$\Sigma_{11}\dot{E}^p_{11} = \frac{1}{h}(1-f)\sigma_M\dot{\sigma}_M \tag{B14}$$

From Equation (B14), $\dot{\sigma}_M$ can be obtained. The consistency condition in Equation (B9) becomes

$$\left[\frac{2\Sigma_{11}}{\sigma_M^2}+2q_1 f\sinh\left(Q_2\frac{\Sigma_{11}}{\sigma_M}\right)\frac{Q_2}{\sigma_M}\right]\dot{\Sigma}_{11}$$
$$-\left[2\frac{\Sigma_{11}^2}{\sigma_M^3}+2q_1 f\sinh\left(Q_2\frac{\Sigma_{11}}{\sigma_M}\right)\frac{Q_2\Sigma_{11}}{\sigma_M^2}\right]\dot{\sigma}_M \tag{B15}$$
$$+\left[2q_1\cosh\left(Q_2\frac{\Sigma_{11}}{\sigma_M}\right)-2q_3 f\right]\dot{f}=0$$

Now $\dot{\Sigma}_{11}$ can be solved from Equation (B15). Once $\dot{\Sigma}_{11}$ is determined, $\dot{E}_{11}^e$ can be determined by Equation (B2). Then $\dot{E}_{11}$ can be determined by Equation (B1). Based on the rate equations discussed earlier, the evolution of the macroscopic stress Σ_{11}, the matrix flow stress σ_M, and the void volume fraction f can be obtained incrementally as a function of E_{11} with the initial conditions of f and $\sigma_M(=\sigma_o)$.

For the uniaxial tensile load applied at 45° with respect to the rolling direction, denote the macroscopic tensile stresses as Σ'_{11} and Σ'_{12}, the macroscopic strains as E'_{11} and E'_{22}. Note that $\Sigma'_{22}=E'_{12}=0$. Based on the stress transformation, $\Sigma_{11}=\frac{1}{2}\Sigma'_{11}-\Sigma'_{12}$, $\Sigma_{22}=\frac{1}{2}\Sigma'_{11}+\Sigma'_{12}$, $\Sigma_{12}=\frac{1}{2}\Sigma'_{11}$, $\Sigma_{23}=\Sigma_{31}=\Sigma_{33}=0$. Based on the strain transformation, $E'_{12}=-\frac{1}{2}E_{11}+\frac{1}{2}E_{22}$. The macroscopic plastic strain rate $\dot{E}_{ij}^p$ can be obtained from the associated flow law as

$$\dot{E}_{11}^p=\dot{\Lambda}\frac{\partial\Phi}{\partial\Sigma_{11}}=\dot{\Lambda}\left[\frac{2\Sigma_{11}+2R_0(\Sigma_{11}-\Sigma_{22})}{(1+R_0)\sigma_M^2}+2q_1 f\sinh\left(Q_2\frac{\Sigma_{11}+\Sigma_{22}}{\sigma_M}\right)\frac{Q_2}{\sigma_M}\right] \tag{B16}$$

$$\dot{E}_{22}^p=\dot{\Lambda}\frac{\partial\Phi}{\partial\Sigma_{22}}=\dot{\Lambda}\left[\frac{\frac{2R_0}{R_{90}}\Sigma_{22}+2R_0(\Sigma_{22}-\Sigma_{11})}{(1+R_0)\sigma_M^2}+2q_1 f\sinh\left(Q_2\frac{\Sigma_{11}+\Sigma_{22}}{\sigma_M}\right)\frac{Q_2}{\sigma_M}\right] \tag{B17}$$

$$\dot{E}_{12}^{p} = \dot{\Lambda}\frac{\partial \Phi}{\partial \Sigma_{12}} = \dot{\Lambda}\left[\frac{(R_0 + R_{90})(2R_{45}+1)}{(1+R_0)R_{90}}\frac{\Sigma_{12}}{\sigma_M^2}\right] \tag{B18}$$

$$\dot{E}_{kk}^{p} = \dot{\Lambda}\frac{\partial \Phi}{\partial \Sigma_{kk}} = \dot{\Lambda}\left[6q_1 f \sinh\left(Q_2\frac{\Sigma_{11}+\Sigma_{22}}{\sigma_M}\right)\frac{Q_2}{\sigma_M}\right] \tag{B19}$$

Manipulate the imposed macroscopic stress, strain conditions and the stress, strain transformations, Σ'_{12} can be expressed as $\frac{\Sigma'_{11}(R_{90}-R_0)}{2(R_0+4R_0R_{90}+R_{90})}$. Therefore, $\Sigma_e = Q_3\Sigma'_{11}$, where $Q_3 = \frac{1}{2}\sqrt{\frac{2R_0R_{90}(3+2R_{45})+(1+2R_{45})(R_0+R_{90})^2+8R_0R_{90}(1+R_{45})(R_0+R_{90})}{R_{90}(1+R_0)(R_0+4R_0R_{90}+R_{90})}}$, and $\Sigma_{kk} = \Sigma_{11}+\Sigma_{22}$. We first solve the initial value of Σ_{11} from the macroscopic yield criterion in Equation (B4) for a given f and σ_M (= σ_o). With the initial conditions, rate equations are needed to determine the evolution of the macroscopic plastic strain rates $\dot{E}_{ij}^{p}$, the matrix flow stress σ_M, and the void volume fraction f.

For a prescribed $\dot{E}_{11}^{p}$, the scalar factor $\dot{\Lambda}$ can be solved from Equation (B16). Once $\dot{\Lambda}$ is solved, $\dot{E}_{22}^{p}$, $\dot{E}_{12}^{p}$, and $\dot{E}_{kk}^{p}$ can be obtained. Once $\dot{E}_{kk}^{p}$ is determined, Equation (B6) gives the growth rate of the void volume fraction, $\dot{f}$. Equation (B8) becomes

$$\Sigma_{11}\dot{E}_{11}^{p} + \Sigma_{22}\dot{E}_{22}^{p} + 2\Sigma_{12}\dot{E}_{12}^{p} = \frac{1}{h}(1-f)\sigma_M\dot{\sigma}_M \tag{B20}$$

Equation (B20) can be used to determine $\dot{\sigma}_M$.

The consistency condition in Equation (B9) becomes

$$\left[\frac{2\Sigma_{11}+2R_0(\Sigma_{11}-\Sigma_{22})}{(1+R_0)\sigma_M^2}+2q_1 f\sinh\left(Q_2\frac{\Sigma_{11}+\Sigma_{22}}{\sigma_M}\right)\frac{Q_2}{\sigma_M}\right]\dot{\Sigma}_{11}$$
$$+\left[\frac{\frac{2R_0}{R_{90}}\Sigma_{22}+2R_0(\Sigma_{22}-\Sigma_{11})}{(1+R_0)\sigma_M^2}+2q_1 f\sinh\left(Q_2\frac{\Sigma_{11}+\Sigma_{22}}{\sigma_M}\right)\frac{Q_2}{\sigma_M}\right]\dot{\Sigma}_{22}$$
$$+2\left[\frac{(R_0+R_{90})(2R_{45}+1)}{(1+R_0)R_{90}}\frac{\Sigma_{12}}{\sigma_M^2}\right]\dot{\Sigma}_{12} \qquad \text{(B21)}$$
$$-\left[2\frac{\Sigma_e^2}{\sigma_M^3}+2q_1 f\sinh\left(Q_2\frac{(\Sigma_{11}+\Sigma_{22})}{\sigma_M}\right)\frac{Q_2(\Sigma_{11}+\Sigma_{22})}{\sigma_M^2}\right]\dot{\sigma}_M$$
$$+\left[2q_1\cosh\left(Q_2\frac{(\Sigma_{11}+\Sigma_{22})}{\sigma_M}\right)-2q_3 f\right]\dot{f}=0$$

Now $\dot{\Sigma}_{11}$ can be solved from Equation (B21) and the stress transformation, $\Sigma_{11}=\frac{1}{2}\Sigma'_{11}-\Sigma'_{12}$, $\Sigma_{22}=\frac{1}{2}\Sigma'_{11}+\Sigma'_{12}$, $\Sigma_{12}=\frac{1}{2}\Sigma'_{11}$. $\dot{E}^e_{11}$, $\dot{E}^e_{22}$, and $\dot{E}^e_{12}$ can then be determined by Equation (B2) when $\dot{\Sigma}_{11}$, $\dot{\Sigma}_{22}$, and $\dot{\Sigma}_{12}$ is determined. Then $\dot{E}_{11}$, $\dot{E}_{22}$, and $\dot{E}_{12}$ can be determined by Equation (B1). Based on the rate equations discussed earlier, the evolution of the macroscopic stress $\dot{\Sigma}_{11}$, $\dot{\Sigma}_{22}$, and $\dot{\Sigma}_{12}$, the matrix flow stress σ_M, and the void volume fraction f can be obtained incrementally as a function of $\dot{E}^p_{11}$ with the initial conditions of f and $\sigma_M(=\sigma_o)$. Based on the stress transformation, as a function of E'_{11} can be obtained.

For the uniaxial tension applied at 90° from the rolling direction case, $\Sigma_{11} = \Sigma_{33} = 0$. Therefore, $\Sigma_e = Q_4\Sigma_{22}$, where $Q_4 = \sqrt{\frac{R_0(1+R_{90})}{(1+R_0)R_{90}}}$, and $\Sigma_{kk} = 3\Sigma_m = \Sigma_{22}$. The numerical procedure is the same as that of the uniaxial tension at 0° from the rolling

direction except that we first solve the initial value of Σ_{22} from Equation (B4) for a given f and σ_M (= σ_o). However, Equation (B10) - (B12) should be modified as

$$\dot{E}_{11}^p = \dot{\Lambda}\frac{\partial \Phi}{\partial \Sigma_{11}} = \dot{\Lambda}\left[\frac{-2R_0\Sigma_{22}}{(1+R_0)\sigma_M^2} + 2q_1 f \sinh\left(Q_2\frac{\Sigma_{22}}{\sigma_M}\right)\frac{Q_2}{\sigma_M}\right] \tag{B22}$$

$$\dot{E}_{22}^p = \dot{\Lambda}\frac{\partial \Phi}{\partial \Sigma_{22}} = \dot{\Lambda}\left[\frac{2R_0(1+R_{90})}{R_{90}(1+R_0)}\frac{\Sigma_{22}}{\sigma_M^2} + 2q_1 f \sinh\left(Q_2\frac{\Sigma_{22}}{\sigma_M}\right)\frac{Q_2}{\sigma_M}\right] \tag{B23}$$

$$\dot{E}_{33}^p = \dot{\Lambda}\frac{\partial \Phi}{\partial \Sigma_{33}} = \dot{\Lambda}\left[\frac{-2R_0}{R_{90}(1+R_0)}\frac{\Sigma_{22}}{\sigma_M^2} + 2q_1 f \sinh\left(Q_2\frac{\Sigma_{22}}{\sigma_M}\right)\frac{Q_2}{\sigma_M}\right] \tag{B24}$$

and Equation (B13) becomes

$$\dot{E}_{kk}^p = \dot{\Lambda}\frac{\partial \Phi}{\partial \Sigma_{kk}} = \dot{\Lambda}\left[6q_1 f \sinh\left(Q_2\frac{\Sigma_{22}}{\sigma_M}\right)\frac{Q_2}{\sigma_M}\right] \tag{B25}$$

Equation (B8) becomes

$$\Sigma_{22}\dot{E}_{22}^p = \frac{1}{h}(1-f)\sigma_M\dot{\sigma}_M \tag{B26}$$

Equation (B9) becomes

$$\begin{aligned}&\left[\frac{2R_0(1+R_{90})\Sigma_{22}}{R_{90}(1+R_0)\sigma_M^2} + 2q_1 f \sinh\left(Q_2\frac{\Sigma_{22}}{\sigma_M}\right)\frac{Q_2}{\sigma_M}\right]\dot{\Sigma}_{22}\\ &-\left[2\frac{{Q_4}^2\Sigma_{22}^2}{\sigma_M^3} + 2q_1 f \sinh\left(Q_2\frac{\Sigma_{22}}{\sigma_M}\right)\frac{Q_2\Sigma_{22}}{\sigma_M^2}\right]\dot{\sigma}_M\\ &+\left[2q_1\cosh\left(Q_2\frac{\Sigma_{22}}{\sigma_M}\right) - 2q_3 f\right]\dot{f} = 0\end{aligned} \tag{B27}$$

For the equal biaxial tension case, $\Sigma_{11} = \Sigma_{22}$ and $\Sigma_{33} = 0$. In this case, $\Sigma_e = \left(\frac{1}{1+R_0}\frac{R_0+R_{90}}{R_{90}}\right)^{1/2}\Sigma_{11} = \left(\frac{1}{1+R_0}\frac{R_0+R_{90}}{R_{90}}\right)^{1/2}\Sigma_{22}$ and $\Sigma_{kk} = 2\Sigma_{11}$. The numerical

procedure is the same as that of the uniaxial tension at 0° from the rolling direction. However, Equation (B10) – (B12) should be modified as

$$\dot{E}_{11}^{p} = \dot{\Lambda}\frac{\partial \Phi}{\partial \Sigma_{11}} = \dot{\Lambda}\left[\frac{2\Sigma_{11}}{\sigma_M^2(1+R_0)} + 2q_1 f \sinh\left(Q_2\frac{2\Sigma_{11}}{\sigma_M}\right)\frac{Q_2}{\sigma_M}\right] \tag{B28}$$

$$\dot{E}_{22}^{p} = \dot{\Lambda}\frac{\partial \Phi}{\partial \Sigma_{22}} = \dot{\Lambda}\left[\frac{R_0}{(1+R_0)R_{90}}\frac{2\Sigma_{11}}{\sigma_M^2} + 2q_1 f \sinh\left(Q_2\frac{2\Sigma_{11}}{\sigma_M}\right)\frac{Q_2}{\sigma_M}\right] \tag{B29}$$

$$\dot{E}_{33}^{p} = \dot{\Lambda}\frac{\partial \Phi}{\partial \Sigma_{33}} = \dot{\Lambda}\left[\frac{-1}{1+R_0}\frac{R_0+R_{90}}{R_{90}}\frac{2\Sigma_{11}}{\sigma_M^2} + 2q_1 f \sinh\left(Q_2\frac{2\Sigma_{11}}{\sigma_M}\right)\frac{Q_2}{\sigma_M}\right] \tag{B30}$$

and Equation (B13) becomes

$$\dot{E}_{kk}^{p} = \dot{\Lambda}\frac{\partial \Phi}{\partial \Sigma_{kk}} = \dot{\Lambda}\left[6q_1 f \sinh\left(Q_2\frac{2\Sigma_{11}}{\sigma_M}\right)\frac{Q_2}{\sigma_M}\right] \tag{B31}$$

Equation (B8) becomes

$$\Sigma_{11}\dot{E}_{11}^{p} + \Sigma_{22}\dot{E}_{22}^{p} = \frac{1}{h}(1-f)\sigma_M\dot{\sigma}_M \tag{B32}$$

Equation (B9) becomes

$$\begin{aligned}
&\left[\frac{2\Sigma_{11}}{(1+R_0)\sigma_M^2} + 2q_1 f \sinh\left(Q_2\frac{2\Sigma_{11}}{\sigma_M}\right)\frac{Q_2}{\sigma_M}\right]\dot{\Sigma}_{11} \\
&+\left[\frac{2R_0\Sigma_{11}}{(1+R_0)R_{90}\sigma_M^2} + 2q_1 f \sinh\left(Q_2\frac{2\Sigma_{11}}{\sigma_M}\right)\frac{Q_2}{\sigma_M}\right]\dot{\Sigma}_{22} \\
&-\left[\frac{2\Sigma_{11}^2}{(1+R_0)\sigma_M^3}\frac{R_0+R_{90}}{R_{90}} + 2q_1 f \sinh\left(Q_2\frac{2\Sigma_{11}}{\sigma_M}\right)\frac{2Q_2\Sigma_{11}}{\sigma_M^2}\right]\dot{\sigma}_M \\
&+\left[2q_1\cosh\left(Q_2\frac{2\Sigma_{11}}{\sigma_M}\right) - 2q_3 f\right]\dot{f} = 0
\end{aligned} \tag{B33}$$

References

Barlat, F., Lege, D. J., and Brem, J. C. (1991), A six-component yield function for anisotropic materials, *Int. J. Plasticity*, **7**, 693.

Barlat, F., Maeda, Y., Chung, K., Yanagawa, M., Brem, J. C., Hayashida, Y., Lege, D. J., Matsui, K., Murtha, S. J., Hattori, S., Becker, R. C. and Makosey, S. (1997), Yield function development for aluminum alloy sheets, *J. Mech. Phys. Solids*, **45**, 1727.

Bassani, J. L. (1977), Yield characterization of metals with transversely isotropic plastic properties, *Int. J. Mech. Sci*., **19**, 651.

Budianski, B. (1984), Anisotropic plasticity of plane-isotropic sheets, in Dvorak, G. J. and Shield, R. T. (eds.), Mechanics of Material Behavior, Elsevier, Amsterdam, p. 15.

Chien, W. Y., Pan, J., and Tang, S. C., (2001), Modified anisotropic Gurson yield criterion for porous ductile sheet metals, *J. Eng. Mater Tech*., **123**, 409.

Gotoh, M. (1977), A theory of plastic anisotropy based on a yield function of fourth order (plane stress state), *Int. J. Mech. Sci*., **19**, 505.

Gurson, A. L. (1977), Continuum theory of ductile rupture by void growth: part I – yield criterion and flow rules for porous ductile media, *J. Eng. Mater. Tech*., **99**, 2.

Hibbitt, H. D., Karlsson, B. I. and Sorensen, E. P. (2001), ABAQUS user manual, Version 6-2.

Hill, R. (1948), A theory of the yielding and plastic flow of anisotropic metals, *Proc Roy. Soc.* (London), **A193**, 281.

Hill, R. (1979), Theoretical plasticity of textured aggregates, *Math. Proc. Camb. Phil. Soc.*, **85**, 179.

Hom, C. L. and McMeeking, R. M. (1989), Void growth in elastic-plastic materials, *J. Appl. Mech*., **56**, 309.

Jeong, H.-Y. and Pan, J. (1995), A macroscopic constitutive law for porous solids with pressure-sensitive matrices and its implications to plastic flow localization, *Int. J. Solids Struct.*, **32**, 3669.

Liao, K.-C, Friedman, P. A., Pan, J. and Tang, S. C. (1998), Texture development and plastic anisotropy of B.C.C. strain hardening sheet metals, *Int. J. Solids Struct.*, **35**, 5205.

Liao, K.-C., Pan, J. and Tang, S. C. (1997), Approximate yield criterion for anisotropic porous ductile sheet metals, *Mech. Mater*., **26**, 213.

Logan, R. W. and Hosford, W. F. (1980), Upper-bound anisotropic yield locus calculations assuming <111> pencil glide, *Int. J. Mech. Sci*., **22**, 419.

Pardoen, T. and Hutchinson, J. W. (2000), An extended model for void growth and coalescence, *J. Mech. Phys. Solids*, **48**, 2467.

Tvergaard, V. (1981), Influence of voids on shear band instabilities under plane strain conditions, *Int. J. Fract*., **17**, 389.

Tvergaard, V. (1982), On localization in ductile materials containing spherical voids, *Int. J. Fract.*, **18,** 237.

Yoon, J. W., Barlat, F. and Dick, R. E. (2000), Sheet metal forming simulation for aluminum alloy sheets, SAE paper no. 2000-01-0774*, Society of Automotive Engineers*, Warrendale, Pennsylvania.

Table Captions

Table 1. Relative uniform normal displacements applied to the faces of the unit cell for different loading conditions with the major principal loading at 0° from the rolling direction.

Table 2. Relative uniform normal displacements applied to the faces of the unit cell for different loading conditions with the major principal loading at 90° from the rolling direction.

Table 3. Material properties of the steel and the aluminum (from Numisheet'93 conference).

Table 4. Relative uniform normal displacements applied to the faces of the unit cell for nearly uniaxial and nearly equal-biaxial conditions when the matrix hardening is considered.

Figure Captions

Figure 1. An element of sheet metal and a Cartesian coordinate system.

Figure 2. (a) A voided unit cell. (b) One eighth of a finite element mesh of the unit cell. Note that a full unit cell is used for computations.

Figure 3. Finite element computational results (symbols) and the results based on the unmodified anisotropic Gurson yield criterion (curves) with the major principal direction of loading at (a) 0° (b) 45° (c) 90° from the rolling direction for the steel and with the major principal direction of loading at (d) 0° (e) 45° (f) 90° from the rolling direction for the aluminum.

Figure 4. Finite element computational results (symbols) and the results based on the modified anisotropic Gurson yield criterion (curves) with the major principal direction of loading at (a) 0° (b) 45° (c) 90° from the rolling direction for the steel and with the major principal direction of loading at (d) 0° (e) 45° (f) 90° from the rolling direction for the aluminum.

Figure 5. The macroscopic stress-strain relations based on the finite element results, and the unmodified and modified anisotropic Gurson yield criterion under nearly uniaxial tensile conditions for the steel: (a) $f = 0.01$, straining direction at 0° (b) $f = 0.01$, straining direction at 45° (c) $f = 0.01$, straining direction at 90° (d) $f = 0.09$, straining direction at 0° (e) $f = 0.09$, straining direction at 45° (f) $f = 0.09$, straining direction at 90°.

Figure 6. The macroscopic stress-strain relations based on the finite element results, and the unmodified and modified anisotropic Gurson yield criterion under nearly uniaxial tensile conditions for the aluminum: (a) $f = 0.01$, straining direction at 0° (b) $f = 0.01$, straining direction at 45° (c) $f = 0.01$, straining direction at 90° (d) $f = 0.09$, straining direction at 0° (e) $f = 0.09$, straining direction at 45° (f) $f = 0.09$, straining direction at 90°.

Figure 7. The macroscopic stress-strain relations based on the finite element results, and the unmodified and modified anisotropic Gurson yield criterion under nearly equal-biaxial tensile conditions for the steel: (a) $f = 0.01$, stress-strain relation in the X_1 direction (b) $f = 0.01$, stress-strain relation in the X_2 direction (c) $f = 0.09$, stress-strain relation in the X_1 direction (d) $f = 0.09$, stress-strain relation in the X_2 direction.

Figure 8. The macroscopic stress-strain relations based on the finite element results, and the unmodified and modified anisotropic Gurson yield criterion under nearly equal-biaxial tensile conditions for the aluminum: (a) $f = 0.01$, stress-strain relation in the X_1 direction (b) $f = 0.01$, stress-strain relation in the X_2 direction (c) $f = 0.09$, stress-strain relation in the X_1 direction (d) $f = 0.09$, stress-strain relation in the X_2 direction.

Table 1. Relative uniform normal displacements applied to the faces of the unit cell for different loading conditions with the major principal loading at 0° from the rolling direction.

	Equal-triaxial	Equal-biaxial	Plane strain	Nearly uniaxial	Nearly pure shear
ΔX_1	1	1	1	1	1
ΔX_2	1	1	0	-1/2	-1
ΔX_3	1	Not prescribed	Not prescribed	Not prescribed	Not prescribed

Table 2. Relative uniform normal displacements applied to the faces of the unit cell for different loading conditions with the major principal loading at 90° from the rolling direction.

	Equal-triaxial	Equal-biaxial	Plane strain	Nearly uniaxial	Nearly pure shear
ΔX_1	1	1	0	-1/2	-1
ΔX_2	1	1	1	1	1
ΔX_3	1	Not prescribed	Not prescribed	Not prescribed	Not prescribed

Table 3. Material properties of the steel and the aluminum (from Numisheet'93 conference).

	Young's modulus (GPa)	Poisson's ratio	Yield stress (MPa)	R_0	R_{45}	R_{90}
Steel	206	0.3	269.5	1.73	1.34	2.24
Aluminum	71	0.33	137.0	0.71	0.58	0.70

Table 4. Relative uniform normal displacements applied to the faces of the unit cell for nearly uniaxial and nearly equal-biaxial conditions when the matrix hardening is considered.

	Nearly uniaxial			Nearly equal-biaxial
	0°	45°	90°	0°
ΔX_1	1	1	Not prescribed	1
ΔX_2	Not prescribed	Not prescribed	1	R_0 / R_{90}
ΔX_3	Not prescribed	Not prescribed	Not prescribed	Not prescribed

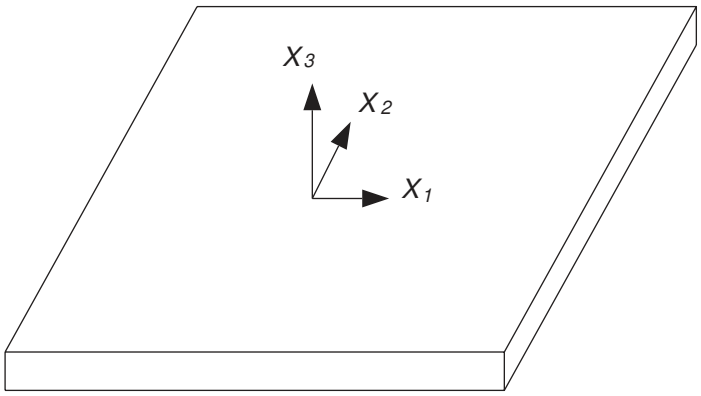

Figure 1. An element of sheet metal and a Cartesian coordinate system.

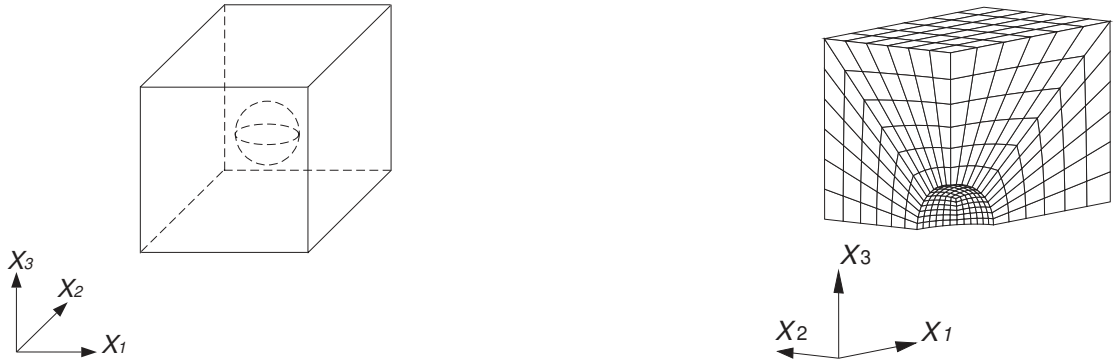

(a) (b)

Figure 2. (a) A voided unit cell. (b) One eighth of a finite element mesh of the unit cell. Note that a full unit cell is used for computations.

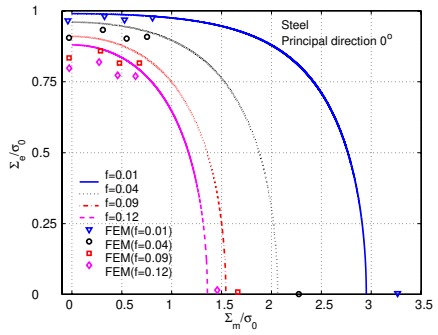

Figure 3(a)

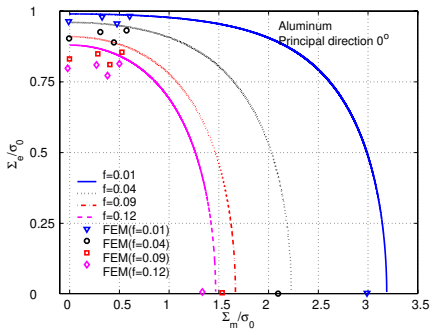

Figure 3(d)

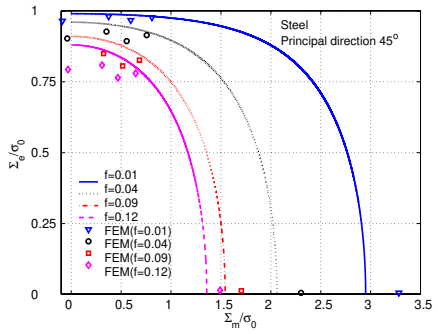

Figure 3(b)

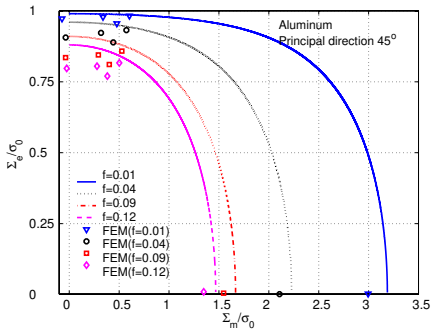

Figure 3(e)

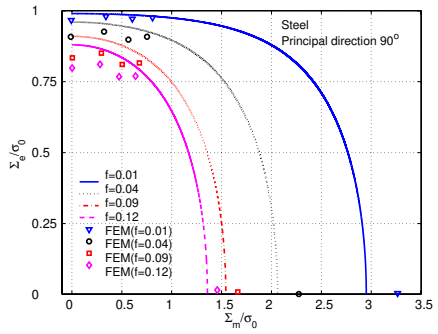

Figure 3(c)

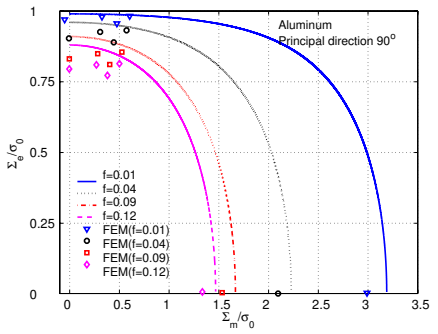

Figure 3(f)

Figure 3. Finite element computational results (symbols) and the results based on the unmodified anisotropic Gurson yield criterion (curves) with the major principal direction of loading at (a) 0° (b) 45° (c) 90° from the rolling direction for the steel and with the major principal direction of loading at (d) 0° (e) 45° (f) 90° from the rolling direction for the aluminum.

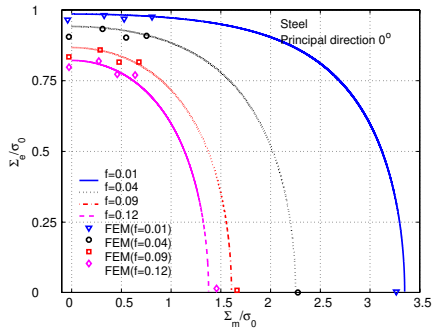

Figure 4(a)

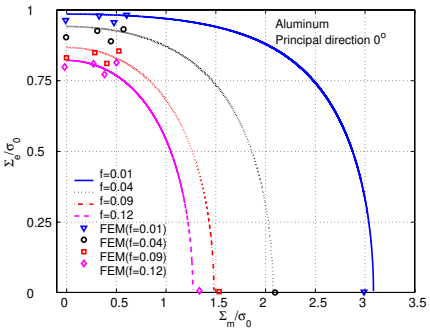

Figure 4(d)

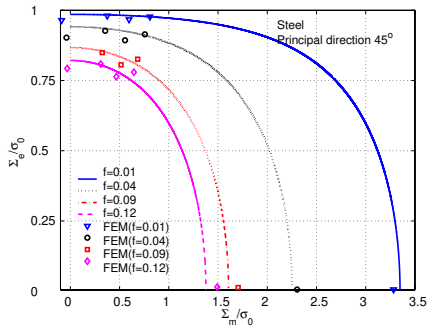

Figure 4(b)

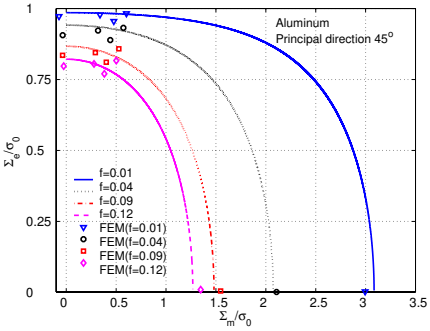

Figure 4(e)

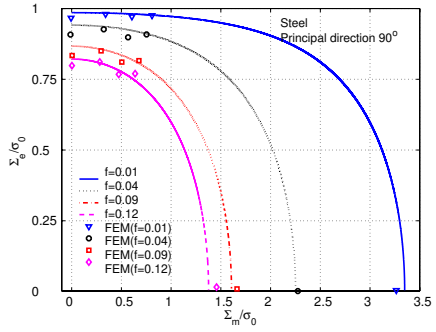

Figure 4(c)

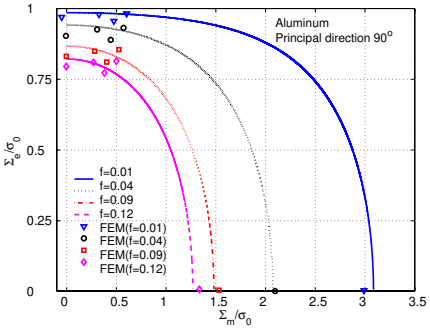

Figure 4(f)

Figure 4. Finite element computational results (symbols) and the results based on the modified anisotropic Gurson yield criterion (curves) with the major principal direction of loading at (a) 0° (b) 45° (c) 90° from the rolling direction for the steel and with the major principal direction of loading at (d) 0° (e) 45° (f) 90° from the rolling direction for the aluminum.

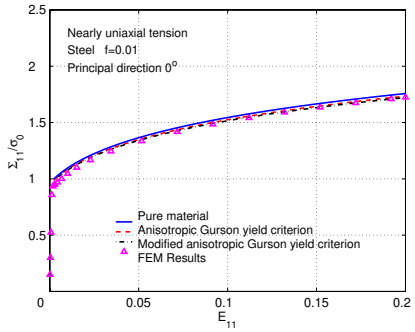

Figure 5(a)

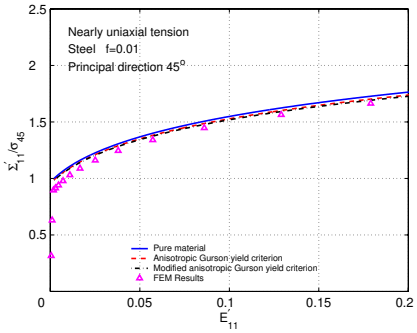

Figure 5(b)

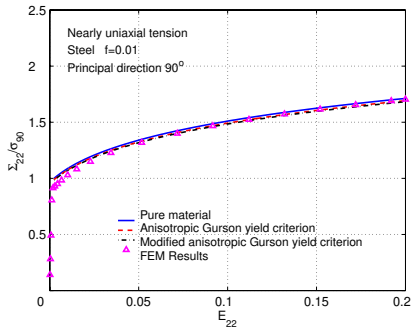

Figure 5(c)

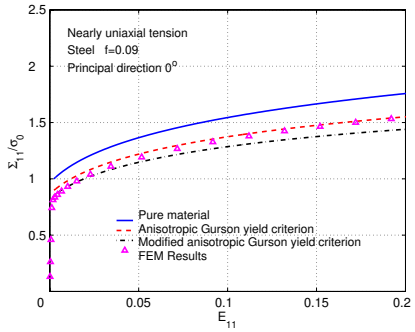

Figure 5(d)

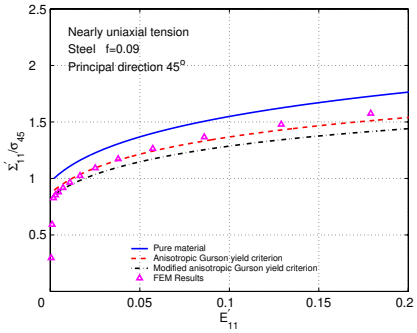

Figure 5(e)

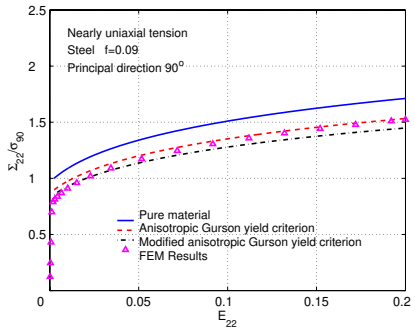

Figure 5(f)

Figure 5. The macroscopic stress-strain relations based on the finite element results, and the unmodified and modified anisotropic Gurson yield criterion under nearly uniaxial tensile conditions for the steel: (a) $f = 0.01$, straining direction at 0° (b) $f = 0.01$, straining direction at 45° (c) $f = 0.01$, straining direction at 90° (d) $f = 0.09$,straining direction at 0° (e) $f = 0.09$, straining direction at 45° (f) $f = 0.09$, straining direction at 90°.

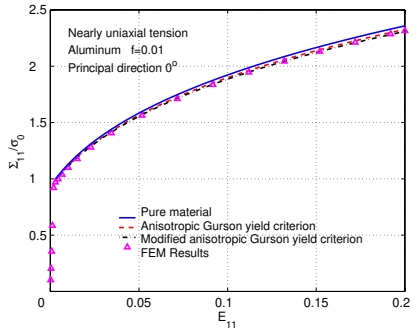

Figure 6(a)

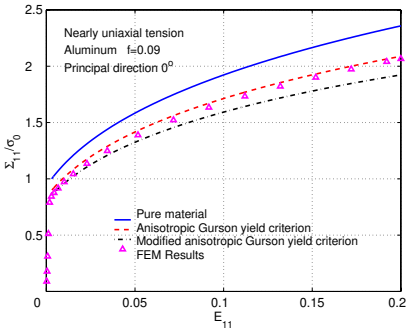

Figure 6(d)

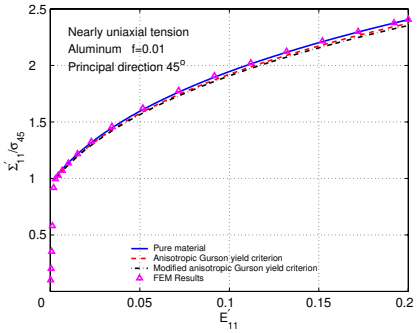

Figure 6(b)

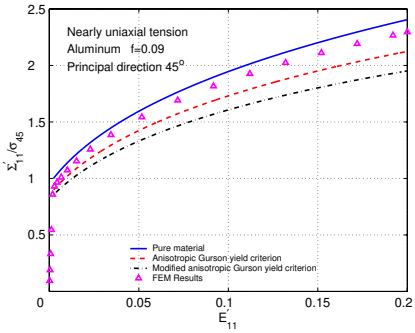

Figure 6(e)

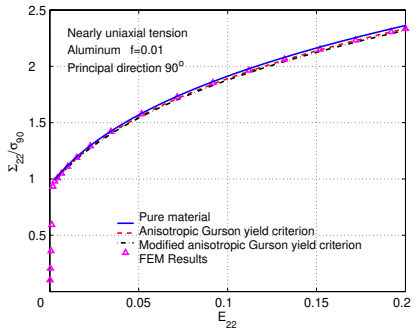

Figure 6(c)

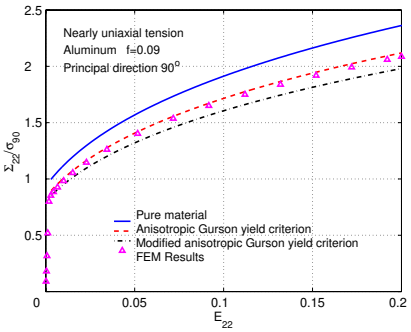

Figure 6(f)

Figure 6. The macroscopic stress-strain relations based on the finite element results, and the unmodified and modified anisotropic Gurson yield criterion under nearly uniaxial tensile conditions for the aluminum: (a) $f = 0.01$, straining direction at 0° (b) $f = 0.01$, straining direction at 45° (c) $f = 0.01$, straining direction at 90° (d) $f = 0.09$, straining direction at 0° (e) $f = 0.09$, straining direction at 45° (f) $f = 0.09$, straining direction at 90°.

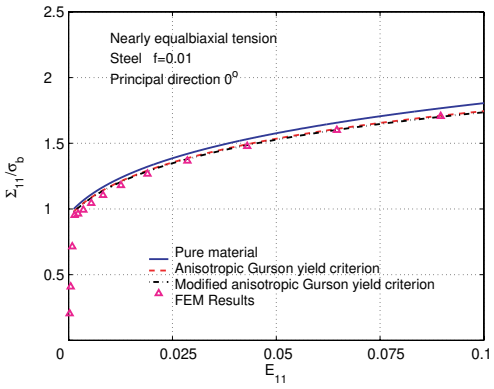

Figure 7(a)

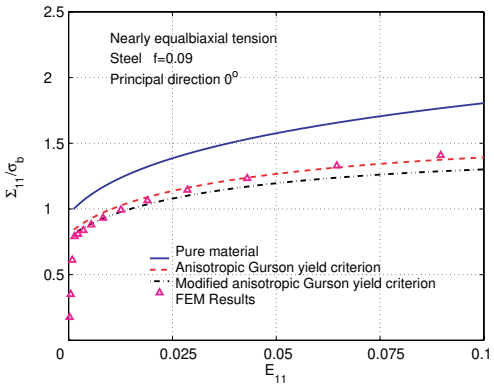

Figure 7(c)

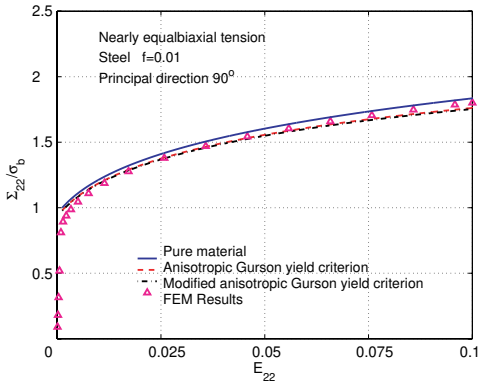

Figure 7(b)

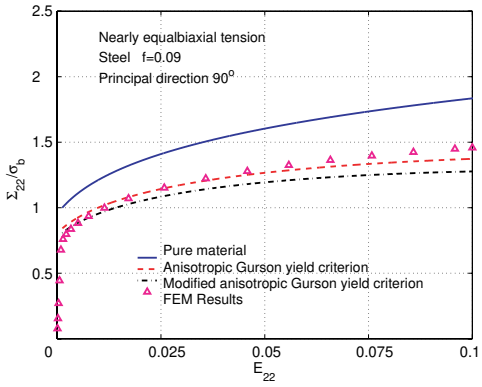

Figure 7(d)

Figure 7. The macroscopic stress-strain relations based on the finite element results, and the unmodified and modified anisotropic Gurson yield criterion under nearly equal-biaxial tensile conditions for the steel: (a) $f = 0.01$, stress-strain relation in the X_1 direction (b) $f = 0.01$, stress-strain relation in the X_2 direction (c) $f = 0.09$, stress-strain relation in the X_1 direction (d) $f = 0.09$, stress-strain relation in the X_2 direction.

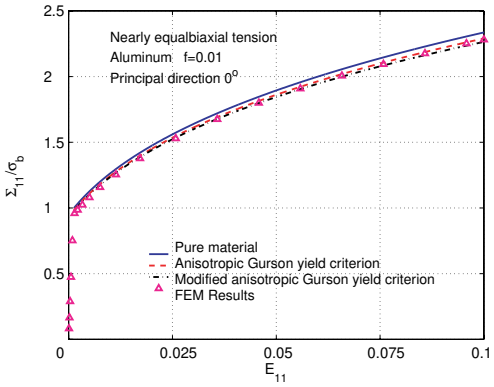

Figure 8(a)

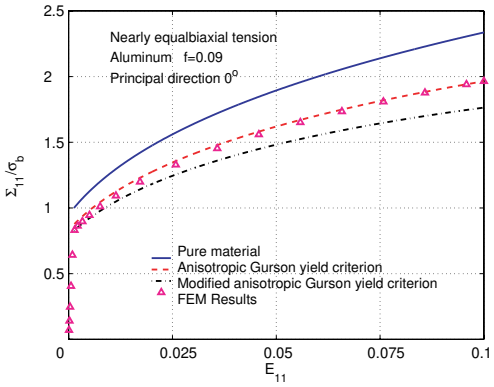

Figure 8(c)

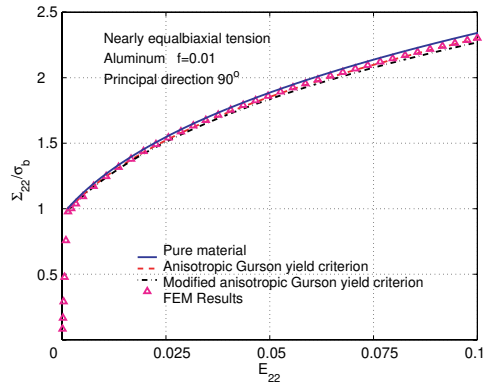

Figure 8(b)

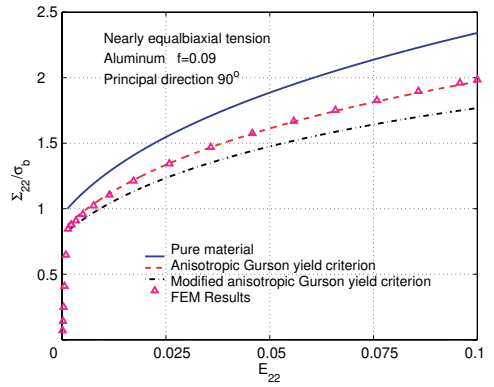

Figure 8(d)

Figure 8. The macroscopic stress-strain relations based on the finite element results, and the unmodified and modified anisotropic Gurson yield criterion under nearly equal-biaxial tensile conditions for the aluminum: (a) $f = 0.01$, stress-strain relation in the X_1 direction (b) $f = 0.01$, stress-strain relation in the X_2 direction (c) $f = 0.09$, stress-strain relation in the X_1 direction (d) $f = 0.09$, stress-strain relation in the X_2 direction.